

The relationship between compression force, image quality and radiation dose in mammography

A Korf, *BMedSc (Hons)*

C P Herbst, *PhD*

W I D Rae, *MB ChB, PhD*

Department of Medical Physics, University of the Free State, Bloemfontein

Abstract

Background. Mammography aims to obtain mammograms of the best possible image quality with the least possible radiation dose. Theoretically, an increase in breast compression gives a reduction in thickness without changing the density, resulting in improved image quality and reduced radiation dose.

Aim. This study investigates the relationship between compression force, phantom thickness, image quality and radiation dose. The existence of a compression point beyond which increased compression gives a change in density rather than thickness is also considered.

Method. Image quality is assessed with a contrast-detail phantom within Superflab phantom on a computed radiography (CR) mammography unit using automatic exposure control (AEC). Image quality is determined by visual inspection and image quality figure (IQF) scoring. The effect of compression and lesion depth on image quality is determined. Entrance and exit doses are calculated. The relationship between entrance dose, compression and thickness is investigated, as is the existence of a compression point beyond which a change in phantom density occurs. The average glandular dose (AGD) is calculated from the scanning average level (SAL) and logarithmic mean (LgM) and compared with the allowable limit.

Results. The geometry effect was not observed. An improvement in image quality with increased compression was found. Entrance dose decreased with increased compression. This trend was not observed with exit dose as AEC was used and exit dose was calculated from SAL values. The 'change-in-density' point of compression was determined. Both LgM and SAL could be used successfully for AGD calculation.

Introduction

The main method of achieving increased image quality and reduced radiation dose is by compression, which spreads out overlapping tissues,¹ gives immobilisation of the breast and decreases exposure time, thus reducing movement. It also decreases breast thickness, whereby the breast dose is reduced. Reduction of the breast dose is important, as the risk of carcinogenesis in the breast is cumulative and directly related to the absorbed breast dose.² Improvement of image quality gives better

visualisation of small lesions and therefore leads to earlier malignancy detection. According to Poulos *et al.*,^{3,4} there exists a point beyond which an increase in compression of the breast does not give spreading of the tissues but rather a change in breast density. Compression beyond this point holds no diagnostic advantage and only contributes to patient discomfort.

The existence of this point is investigated using the Superflab phantom to a maximum compression of 18 decaNewtons (daN) by using Equation 1, where I_0 is the entrance dose, I is the exit dose, μ is the attenuation coefficient and t is the thickness.

$$I = I_0 e^{-\mu t} \quad (1)$$

If the natural logarithm of $\frac{I}{I_0}$ is plotted against thickness t , the slope of the graph is μ and thus a change in the slope of the graph implies a change in μ , which is indicative of a change in density.

With the contrast-detail phantom, image quality is investigated both visually and by image quality figure (IQF) scoring. Contrast is determined in terms of object diameter by detecting pairs of low-contrast objects. The scoring is done according to Equation 2.⁵

$$IQF = \sum_{i=1}^{16} C_i \times D_{i,min} \quad (2)$$

where IQF is the image quality figure, C_i is the radiation contrast for the i^{th} column and $D_{i,min}$ is the threshold diameter in the i^{th} contrast column.

According to Koen *et al.*,⁶ the average glandular dose (AGD) can be calculated from the scanning average level (SAL) and logarithmic mean (LgM) using Equations 3 and 4.

$$AGD(mGy) = 395.71 \times 10^{-6} \times kV^{-1.623} \times SAL^2 \quad (3)$$

$$AGD(mGy) = 4.1693 \times kV^{-1.6865} \times e^{2.329 \times LgM} \quad (4)$$

The AGD must be less than 3 mGy per exposure, according to the American College of Radiology (ACR) manual.⁷

Material and method

A GE Senographe unit was used. Quality assurance of the unit was done according to the specifications in the ACR manual before the study was conducted.

Breast dose was affected by the tube voltage (kVp) and the current-time product (mAs).⁵ These factors were selected by using automatic exposure control (AEC) as this was most commonly used in the facility.

A phantom of Superflab with uncompressed thickness of 60 mm and a minimum thickness of 44 mm was used. This thickness and mate-

Table I. Superflab thickness accuracy and reproducibility at different compression forces

Applied compression force (daN)	0			5			10			15			18		
Displayed thickness (mm)	60	59	60	50	49	50	48	47	47	46	45	45	45	45	44
Actual thickness (mm)	58	57	58	49	48	49	48	48	48	47	46	46	43	44	44
Average displayed thickness (mm)	60			50			47			45			45		
Average actual thickness (mm)	58			49			48			46			44		
Displayed thickness standard deviation (mm)	0.6			0.6			0.6			0.6			0.6		
Actual thickness standard deviation (mm)	0.6			0.6			0.0			0.6			0.6		
Difference between displayed and actual averages (mm)	2.0			1.0			0.7			1.0			1.0		
Standard deviation in difference (mm)	0.8			0.8			0.6			0.8			0.8		
t-test result for displayed and actual thickness	0.01			0.10			0.18			0.10			0.10		

Table II. Entrance and exit dose calculation parameters

Entrance dose parameters					
kV	mAs	mR	mR/mAs	Target/filter	
30	20	1342	67.1	Rh/Rh	
31	20	1471	73.6	Rh/Rh	
32	20	1589	79.5	Rh/Rh	
33	20	1729	86.5	Rh/Rh	
34	20	1870	93.5	Rh/Rh	
35	20	2012	100.6	Rh/Rh	
36	20	2153	107.7	Rh/Rh	
37	20	2297	114.9	Rh/Rh	
38	20	2443	122.2	Rh/Rh	
39	20	2594	129.7	Rh/Rh	
40	20	2747	137.4	Rh/Rh	
Exit dose parameters					
kV	mAs	mR	Exit dose (mGy)	SAL (arb. unit)	Target/filter
31	12.5	0.1	7.0E-04	436	Rh/Rh
31	14.0	0.1	8.0E-04	458	Rh/Rh
31	16.0	0.1	9.0E-04	489	Rh/Rh
31	18.0	0.1	1.1E-03	523	Rh/Rh
31	20.0	0.1	1.1E-03	548	Rh/Rh
31	22.5	0.1	1.3E-03	578	Rh/Rh
31	25.0	0.2	1.4E-03	607	Rh/Rh
31	28.0	0.2	1.7E-03	651	Rh/Rh
31	32.0	0.2	1.8E-03	688	Rh/Rh
31	36.0	0.2	2.1E-03	743	Rh/Rh
31	40.0	0.3	2.3E-03	774	Rh/Rh
31	45.0	0.3	2.6E-03	821	Rh/Rh

rial was selected, as it was comparable to the average compressed and uncompressed thickness of a moderately sized breast.

Compressing the Superflab to 0, 5, 10, 15 and 18 daN and noting the displayed thickness on the mammography unit and actual thickness measured with a ruler, tested the accuracy and reproducibility of the

thickness of the Superflab at different compressions. Measurements were made 3 times at each compression force.

A graph of kV versus mR/mAs was plotted for the calculation of entrance dose from exposure parameters. For this, the kV was varied from 30 - 40 kV and the mAs was set to 20 mAs. A NERO mAx detec-

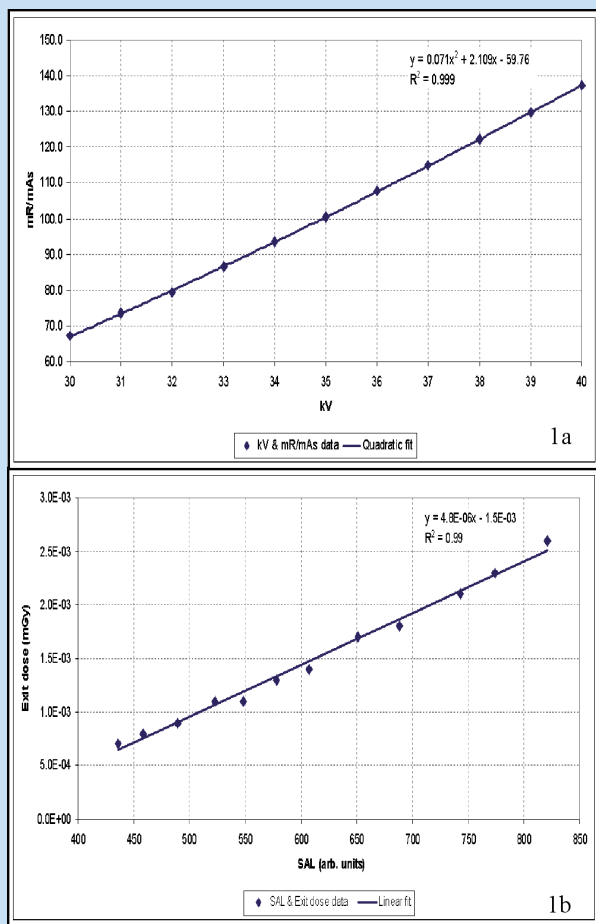


Fig. 1a (above). Entrance dose calculation from kV, mAs and entrance exposure.
Fig. 1b (below). Exit dose calculation from SAL.

tor was used for the measurements on the bucky, i.e. at breast level. The mR/mAs was found to be linear over the range of 5 - 320 mAs.

The exit dose was determined by obtaining the scanning average level (SAL) values of images at different mAs settings, from 12.5 - 45 mAs, at 31 kV, with a 5 cm Perspex attenuator in the beam. Dose measurements were done with a Fluke Biomedical 451 Victoreen ionisation chamber survey meter. A Perspex thickness of 5 cm was selected as this was almost equivalent to an average 6 cm-thick breast, taking density into account. The 5 cm of Perspex reduced the amount of radiation incident on the detector in order to achieve a linear relationship between SAL and exit dose. Exit dose was then determined from the SAL of an image using this relationship. With the contrast-detail phantom at a depth of 6 cm (i.e. the theoretically best geometrical location), AEC exposures for entrance and exit dose calculations were made at compressions of 3 - 18 daN.

The relationship between the calculated entrance dose and phantom thickness, and that between compression force and phantom thickness, were graphically investigated for the Superflab phantom. The existence of a compression force point beyond which an increase in compression gave a change in density was examined using Equation 1.

An Artinis contrast detail mammography (CDMAM)-phantom type 3.4 was used for image quality assessment. The phantom was placed at 0, 2, 4 and 6 cm uncompressed depth in the Superflab for determination of the influence of object depth on image quality, i.e. the geometry effect. At each depth, AEC was used for exposure parameter selection, and different compression forces (3, 10 and 14 daN) were applied.

Geometry effect assessment was done by image quality figure (IQF) scoring of the images at different phantom depths and a constant compression force of 14 daN. Scoring the images obtained at a depth of 6 cm at different compressions assessed the relationship between image quality and compression force. Scoring was done according to Equation 2, and results were compared with theory.

Table III. Contrast-detail phantom imaging parameters

Image number	Imaging parameters			Exposure parameters			LgM (arb. units)	SAL (arb. units)
	Phantom depth (cm)	Compression force (daN)	Phantom thickness (mm)	kV	mAs	Target/filter		
1	0	3	54	32	238	Rh/Rh	2.14	1165
2	0	10	50	32	220	Rh/Rh	2.17	1202
3	0	14	47	32	211	Rh/Rh	2.16	1181
4	2	3	54	32	241	Rh/Rh	2.16	1151
5	2	10	49	32	222	Rh/Rh	2.14	1164
6	2	14	47	32	213	Rh/Rh	2.15	1160
7	4	3	53	32	236	Rh/Rh	2.17	1180
8	4	10	49	32	223	Rh/Rh	2.16	1164
9	4	14	47	32	218	Rh/Rh	2.16	1154
10	6	3	55	32	242	Rh/Rh	2.16	1149
11	6	10	49	32	222	Rh/Rh	2.19	1191
12	6	14	47	32	209	Rh/Rh	2.16	1152
						Average	2.16	1168
						Standard deviation	0.01	16.34

Image quality was visually inspected for the 12 films of the Superflab phantom. The images were ranked from best to worst. The results obtained were compared with the IQF results and with what was expected from theory.

The images obtained on the Agfa CR MM3.0 Mammo CR plates were read with an Agfa CR 85-X reader, and the SAL was obtained in a 10x10 cm² region of interest positioned 4 cm from the chest wall edge and centred laterally. The LgM was automatically calculated for each exposure. The SAL and LgM were used to calculate the AGD according to Equations 3 and 4. The results were compared with the ADG limit of 3 mGy per exposure.⁷

With each exposure, the kVp, mAs, target/filter combination, SAL, LgM, compression force and displayed phantom thickness were noted.

Results

The accuracy and reproducibility of the thickness of the Superflab at different compressions was investigated and the results noted in Table I.



Fig. 2. CDMAM Superflab phantom image.

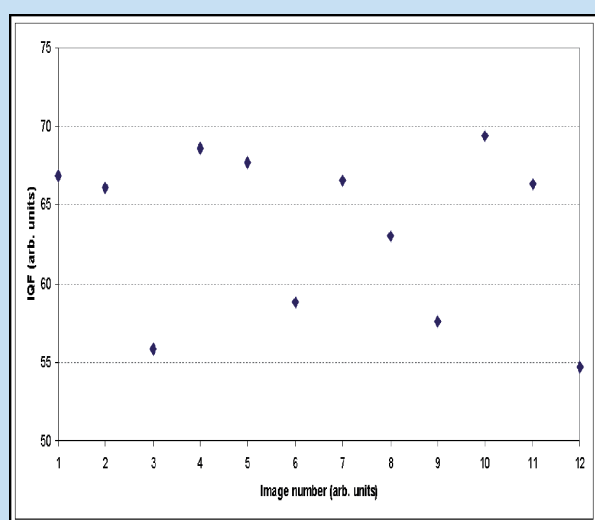


Fig. 3. IQF scoring demonstrating the geometry effect, compression force and image quality relationship.

The results for entrance and exit dose calculation are shown in Table II. Fig. 1a was plotted from the entrance dose data in Table II, and Fig. 1b shows the relationship between exit dose and SAL.

The contrast-detail phantom was imaged in the Superflab at different depths and compressions, and the results tabulated in Table III. An example of the images that were obtained is shown in Fig. 2.

The 12 films of the Superflab phantom were ranked visually. Image 1 was the theoretically best image, i.e. the image obtained with the contrast-detail phantom at 6 cm depth and a 14 daN compression force. Image 12 was the theoretically worst image, i.e. with the phantom at 0 cm depth and 3 daN compression. The theoretical classification of the images, the visual ranking positions and the IQF scoring results appear in Table IV.

The stability of the LgM and SAL values of the different images was investigated statistically and the results shown in Table III.

The geometry effect was assessed by looking at the image quality at a certain compression force (14 daN) at different phantom depths, i.e. 0, 2, 4 and 6 cm. The relationship between image quality and compression force was investigated by considering image quality at a certain depth, i.e. 6 cm, for different compression forces, i.e. 3, 10 and 14 daN. This is shown in Fig. 3 in terms of the IQF of the different images.

For the dosimetry analysis, the exposure parameters and results were recorded in Table V. Here, the equation of the quadratic fit on Fig. 1a and the AEC kV and mAs were used to calculate the entrance exposures in mR, which was converted to entrance dose. The AGD values calculated with Equations 3 and 4 were compared statistically. The comparison is included in Table V.

The relationship between entrance dose and phantom thickness, and the correlation between compression force and phantom thickness, are shown in Fig. 4.

A graph of the natural logarithm of the quotient of the exit dose by the entrance dose against the thickness of the phantom (see Fig. 5a) was used to determine the 'change-in-density' point where an increase in compression resulted in changed density. Fig. 5b shows a plot of the slope (i.e. μ) of Fig. 5a.

The AGD values calculated with Equations 3 and 4 were compared statistically. The results are set out in Table V.

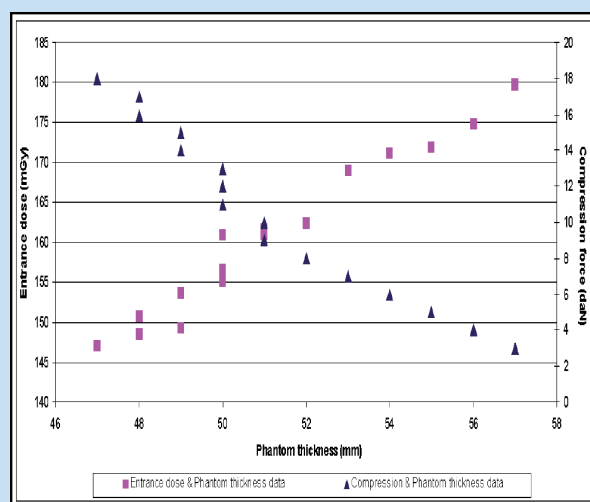


Fig. 4. Entrance dose and compression force.

Discussion

Table I indicates that the thickness of the Superflab, as displayed on the unit and measured with a ruler, was accurate and reproducible. Standard deviations were very small. There was no significant difference between the actual and displayed thickness values. The *t*-test results showed that the null hypothesis (i.e. that the actual and displayed thickness values

were the same) could not be rejected with authority. The displayed thickness was therefore used for the rest of the study.

Theoretically, the SAL and LgM values should remain similar for different exposures when AEC is used. We found that the values were tightly grouped around the mean values, i.e. the standard deviations were small, as shown in Table III.

Table IV. Different Superflab phantom image classifications

Image number	Imaging parameters		Theoretical classification position	Visual inspection classification position	IQF scoring position
	Compression force (daN)	Phantom depth (cm)			
12	14	6	1	2	1
11	10	6	2	6	8
10	3	6	3	10	12
9	14	4	4	4	3
8	10	4	5	8	5
7	3	4	6	12	9
6	14	2	7	1	4
5	10	2	8	5	10
4	3	2	9	9	11
3	14	0	10	3	2
2	10	0	11	7	7
1	3	0	12	11	6

Table V. Dosimetry analysis results

Compression force (daN)	kV	mAs	Phantom thickness (mm)	Calculated mR/mAs	Calculated entrance exposure (mR)	Calculated entrance dose, I ₀ (mGy)	Calculated exit dose, I (mGy)	ln (I/I ₀) (arb. units)	LgM from image	SAL from image	ln(I/I ₀)/phantom thickness (arb. units)	AGD (mGy) from LgM	AGD (mGy) from SAL
3	32	247	57	79.9	19736.3	179.8	3.26E-03	10.9	2.15	952	0.19	1.8	1.3
4	32	240	56	79.9	19177.0	174.7	3.16E-03	10.9	2.13	932	0.20	1.7	1.2
5	32	236	55	79.9	18857.4	171.8	3.16E-03	10.9	2.12	932	0.20	1.7	1.2
6	32	235	54	79.9	18777.5	171.1	3.18E-03	10.9	2.12	935	0.20	1.7	1.2
7	32	232	53	79.9	18537.8	168.9	3.22E-03	10.9	2.12	944	0.21	1.7	1.3
8	32	223	52	79.9	17818.6	162.3	3.16E-03	10.8	2.11	932	0.21	1.6	1.2
9	32	222	51	79.9	17738.7	161.6	3.21E-03	10.8	2.11	942	0.21	1.6	1.3
10	32	221	51	79.9	17658.8	160.9	3.16E-03	10.8	2.11	931	0.21	1.6	1.2
11	32	221	50	79.9	17658.8	160.9	3.29E-03	10.8	2.12	957	0.22	1.7	1.3
12	32	215	50	79.9	17179.4	156.5	3.25E-03	10.8	2.11	950	0.22	1.6	1.3
13	32	213	50	79.9	17019.6	155.0	3.14E-03	10.8	2.10	928	0.22	1.6	1.2
14	32	211	49	79.9	16859.8	153.6	3.25E-03	10.8	2.12	949	0.22	1.7	1.3
15	32	205	49	79.9	16380.4	149.2	3.18E-03	10.8	2.10	936	0.22	1.6	1.3
16	32	204	48	79.9	16300.5	148.5	3.25E-03	10.7	2.11	950	0.22	1.6	1.3
17	32	207	48	79.9	16540.2	150.7	3.28E-03	10.7	2.12	955	0.22	1.7	1.3
18	32	202	47	79.9	16140.6	147.0	3.25E-03	10.7	2.12	969	0.23	1.7	1.3
Average												1.7	1.3
Standard deviation												0.05	0.03
<i>t</i> -test result for AGD												3.8E-21	

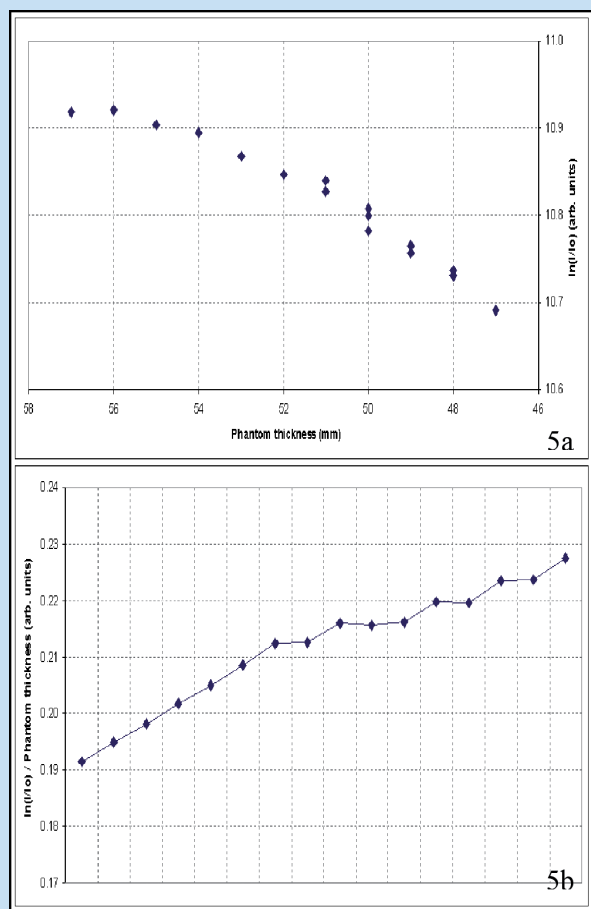


Fig. 5. Determining compression 'change-in-density' point. Fig. 5a (above): Phantom thickness versus $\ln(I/I_0)$ with μ the slope of the graph. Fig. 5b (below): Line graph of μ .

Table IV demonstrates that visual classification of the images yielded no well-defined pattern. The images were not ranked according to what was expected from theory, which meant that distinct variations in image quality between the 12 images were not seen, and implied that increased compression and lesion depth did not influence visual image quality to a great extent.

One would expect that image quality should improve as the contrast-detail phantom was placed closer to the image receptor, owing to the geometry effect. The quality should also be better with greater compression force. When the IQF of the Superflab phantom was considered, Fig. 3 indicated that the compression force did affect image quality considerably. On the figure, groups of images were distinguished, i.e. images 1 - 3, 4 - 6, 7 - 9 and 10 - 12, as obtained with the contrast-detail phantom at a depth of 0, 2, 4 and 6 cm respectively. Within a group, the images were acquired at 3, 10 and 14 daN compression. For all the image groups, the IQF of the images became smaller as the compression force was increased; thus, the image quality improved. However, when the images obtained at a certain compression force at different depths of the contrast-detail phantom were compared, such a trend was not observed. The geometry effect was thus not shown. This result was in accordance

with that of Poulos *et al.* who showed that if minimisation of breast thickness were not done, image quality would be compromised and the potential to miss small lesions would increase.⁴

The quadratic relationship between kV and mR/mAs (or dose) of Fig. 1a was used to calculate the entrance exposure mR at a certain kV and mAs. A Roentgen-to-rad conversion factor of 0.911, as recommended by Khan,⁸ was used. The peak energy of the beam was 31keV, therefore the average energy was approximately a third, i.e. 10keV. According to Khan, one Roentgen equalled 0.911 rad in water at this average energy. This answer was multiplied by 10 to convert to mGy. The correspondence between exit dose in mGy and the SAL of an image was obtained from the Fig. 1b equation.

Fig. 4 demonstrates that entrance dose decreased as phantom thickness decreased, i.e. as compression force was increased, which was a main argument in increasing compression as much as possible. Increased compression gave reduced phantom thickness; however, continuous spreading of phantom tissue was not achieved and density was changed. This was further indicated in Fig. 5.

The point of compression beyond which the density of the phantom was changed, with decreased tissue spreading, can be determined from Fig. 5. From the equation of a straight-line graph, μ was the gradient, and it should have remained constant if continuous spreading of tissues and reduction in phantom thickness was achieved without changing the density. This implied that Fig. 5a should have been a linear graph and Fig. 5b a horizontal line graph. It was therefore clear that a 'change-in-density' compression point did exist and that the density of the Superflab changed with increased compression.

Poulos *et al.*³ advised that compression should only be applied until the minimum breast thickness was achieved and not beyond that point, and that a large number of women did not have a change in breast thickness with reduced compression; this implied no benefit with increased discomfort. We made the same finding in this study.

The calculated AGD values in Table V were relatively stable for each method of calculation, but the results of the two calculation methods differed somewhat. However, the *t*-test proved that the null hypothesis that the AGD calculated with the SAL and LgM were the same could not be rejected with confidence. The AGD values were also closely grouped around the mean value, showing that the dose with AEC stayed repeatedly constant. All the calculated AGD values were less than the limit of 3 mGy.

With the Superflab phantom, visual arrangement and IQF scoring of images obtained at different compression forces did not rank the images according to theoretical predictions. Lesion detection would be improved with increased compression for a lesion situated at a certain depth. We found that lesions or calcifications situated closer to the image receptor did not have a better chance of being detected owing to the geometry effect.

The aim in mammography should be minimisation of breast thickness rather than maximisation of breast compression.⁶ In our study, it was shown that minimisation of phantom thickness resulted in improved image quality, increased chance of detection of small lesions, and reduced radiation dose. Increasing compression gave reduced phantom thickness up to a point after which no image quality benefits were achieved, entrance dose still decreased, and patient discomfort

increased. This was an important finding because discomfort and pain discourage women from having regular mammograms. By not over-compressing a breast beyond the 'change-in-density' point, pain could be reduced without much reduction in image quality.

In response to the aim of our study, we found that a trade-off existed between increased compression force, reduced phantom thickness, improved image quality, reduced radiation dose, and increased patient discomfort. Early lesion detection remained the primary objective; therefore, from the results of this study, it is recommended that breast compression is done up to the point of maximum displacement of breast tissue, but not beyond. We also concluded that less compression was acceptable, without a significant reduction in visual image quality, if the woman was uncomfortable or experienced pain.

The primary goal of compression is reduction in breast thickness, which leads to reduced scatter and in turn better image quality. Reduced radiation dose is a secondary benefit. With the Superflab phantom, we found that entrance dose continued to decrease although image quality was not improved when the density of the phantom was changed. If

reduced dose were the primary objective of compression, maximisation of compression would have been the aim, but image quality was the main aim and therefore minimisation of breast thickness is recommended.

We thank the personnel of the Mammography Division of the Diagnostic Radiology Department at Universitas Hospital, Bloemfontein, for accommodating our study.

1. Saunders RS, Samei E. The effect of breast compression on mass conspicuity in digital mammography. *Med Phys* 2008; 35(10): 4464-4473.
2. Brnić Z, Hebrang A. Breast compression and radiation dose in two different mammographic oblique projections: 45 and 60°. *Eur J Radiol* 2001; 40(1): 10-15.
3. Poulos A, McLean D, Rickard M, Heard R. Breast compression in mammography: How much is enough? *Australas Radiol* 2003; 47: 121-126.
4. Poulos A, McLean D. The application of breast compression in mammography: a new perspective. *Radiography* 2004; 10(2): 131-137.
5. Thijssen MAO, Bijkerk KR, van der Burght RJM. *Manual contrast-detail phantom Artinis CDMAM type 3.4*. Zetten, The Netherlands: Artinis Medical Systems B.V., 2007.
6. Koen I, Herbst CP, Rae WID. Computed radiography exposure indices in mammography. *South African Journal of Radiology* 2008; 28-31.
7. *Mammography Quality Control Manual*, revised ed. Reston, USA: American College of Radiology, 1994.
8. Khan FM. *The Physics of Radiation Therapy*. Baltimore: Lippincott Williams and Wilkins, 1984: 110-112.